PAPER

Check for updates

DNA-binding, antioxidant, H$_2$O$_2$ sensing and photocatalytic properties of biogenic silver nanoparticles using *Ageratum conyzoides* L. leaf extract

Sandip Kumar Chandraker, Mishri Lal and Ravindra Shukla [iD] *

Green nanotechnology is gaining widespread interest owing to the elimination of harmful reagents and offers a cost-effective synthesis of expected products. In the present study, silver nanoparticles (AgNPs) were synthesized from *Ageratum conyzoides* leaf extract (ACLE). UV-visible spectrophotometry showing a characteristic SPR peak at 443 nm verified the phytosynthesis of AC-AgNPs. The FTIR spectrum was examined to identify the efficient functional molecules responsible for the reduction of Ag$^+$ to metallic silver (Ag^0). SEM, TEM and XRD illustrated the formation of crystalline and spherical NPs with a size range of 14–48 nm. EDX data showed the presence of elemental silver with an energy peak at 3 eV. CT-DNA interaction with AC-AgNPs was investigated and the UV absorption spectra revealed a bathochromic effect indicating groove binding. AC-AgNPs showed a strong antioxidant property in a concentration-dependent manner when analyzed by DPPH and ABTS radical scavenging assay. AC-AgNPs were investigated as a SPR-based H$_2$O$_2$ sensor, which can provide promising opportunities in medical and environmental fields to detect reactive oxygen species such as H$_2$O$_2$. The catalytic effectiveness of phytosynthesized NPs was also examined within 2 h of exposure for methylene blue degradation under sunlight. There is thus a reasonable potential application of green synthesized AC-AgNPs for the degradation of hazardous synthetic dyes.

1. Introduction

Nanotechnology is an interdisciplinary and most attractive area of research in recent years. It has influenced every dimension of science, economy and all life steps that include the design, synthesis and manipulation of nano-sized materials in multiple ways. Nanoparticles have various applications regarding biological and medicinal aspects such as catalytic activity, water purification, chemical and biological sensors, wireless electronic logic and memory schemes.[1] They have a very significant role in the material sciences owing to their defined size, shape, optical, mechanical and biological properties.[2] Due to the small size range of nanoparticles (1–100 nm), they provides a high surface area and reactivity which makes them popular in biomedicine for therapeutic purposes.[3]

Biological route of nanoparticle synthesis is free from the use of hazardous chemicals or irradiations and preferred over physical and chemical methods. The plant-mediated green synthetic approach of nanoparticle is greatly advantageous over microbial synthesis as the process is highly economical

compared to the cost of microorganism isolation and their culture maintenance.[4,5] The phytosynthesis of nanoparticles is rapid, low cost, eco-friendly, and one-step method.[6] Since the plant extracts contain various secondary metabolites such as alkaloids, flavonoids, saponins, steroids, tannins, *etc.*, it acts as a reducing and stabilizing agent for the bioreduction reaction to synthesize novel metallic nanoparticles. AgNPs synthesis is a promising field of research and much needed because nano-scale silver has shown entirely distinct characteristics to bulk particles made of the same material.[7]

In recent years, studies on interaction of metal NPs with DNA are of primary concern due to its possible effect on the structural integrity and synthesis of DNA.[8] Several methods like gel electrophoresis, electrochemical techniques and UV-vis spectroscopy have been employed to elucidate interaction of tiny molecules with DNA. However, spectroscopic techniques are convenient, accurate and highly sensitive compared to other complicated methods.[9]

H$_2$O$_2$ is a strong oxidizing agent which is widely used in the food, pharmaceutical, cosmetics, wood and pulp industries. However, the exposure and presence of even a small amount of H$_2$O$_2$ in process streams result in various health and environmental hazards due to its toxicity.[10] It is therefore, essential to develop accurate, stable and fast methods to detect H$_2$O$_2$ residue

Laboratory of Bio-resource Technology, Department of Botany, Indira Gandhi National Tribal University, Amarkantak-484887, Madhya Pradesh, India. E-mail: ravindra. shukla@igntu.ac.in; Tel: +91-8656-948490

in commercially available products. Chemiluminescence, optical detection and electrochemical methods have been developed for the sensitive determination of H_2O_2.[11] AgNPs based non-enzymatic sensor for H_2O_2 has been developed by electrodeposition method and by using *Bacillus subtilis*.[12,13] Only few reports are available on phytosynthesized AgNPs for H_2O_2 sensing capacity using *Calliandra haematocephala*, *Lavandula officinalis*, *Lithodora hispidula*, *Mangifera indica* etc.[11,14–16]

Synthetic dyes are a potential hazard to living organisms produced by textile, paper, food, cosmetics, and pharmaceutical industries. These causes serious health and ecological problems, and some of them have exhibited mutagenic and carcinogenic effects.[17] Methylene blue (MB) is a synthetic thiazine dye used as a traditional colorant in the textile and paint industries. However, proven as an industrial pollutant, its odor, and direct contact may cause allergic reactions, burning of skin and eyes, breathlessness, vomiting, *etc.*[18] Different methods commonly adopted for detoxification of dyes using UV radiations, toxic stabilizers, solvents, surfactants, flocculation, redox treatments and microbial biodegradation.[15] These techniques are inefficacious and require a better approach. Catalytic degradation under visible-light irradiation has gained widespread attention because it is rapid, highly efficient and economical, and does not cause secondary pollution.[19]

Ageratum conyzoides L. (family: Asteraceae) in an invasive weed of Indo-Gangetic plains and Narmada basin, and abundantly found in and around Indian agro-ecosystems. The plant has morphological variations and highly adaptable to different ecological conditions. A number of chemical compounds including alkaloids, flavonoids, chromenes, benzofurans and terpenoids have been isolated from this species.[20] Extracts and metabolites from this plant has been found to possess hypoglycemic, anti-inflammatory, antifungal, antimalarial, antiprotozoal and insecticidal activities.[21]

The objectives of the present study were to synthesize and characterize the AgNPs using the aqueous leaf extract of *A. conyzoides*. In addition, DNA binding, free radical scavenging, photo-catalytic degradation of MB and H_2O_2 sensing properties of AgNPs were also investigated.

2. Materials and methods

2.1 Plant materials

The leaves of *A. conyzoides* were collected during September 2018 from Keonchi region of Achanakmar Amarkantak Biosphere Reserve under Bilaspur District, Chhattisgarh State, India. The authentication of plant species was done by subject experts, and a voucher specimen (DOB/07/AC/043) deposited in Department of Botany, Indira Gandhi National Tribal University, Amarkantak, India.

2.2 Preparation of leaf extract and biosynthesis of AgNPs

The collected fresh leaves of *A. conyzoides* were washed thoroughly with tap water and twice with Milli-Q water to eliminate the organic impurities, and dust present on it. The extract was prepared with 10 g of fresh leaves that were uniformly cut into small pieces. Chopped leaves were boiled for 15 min in 100 mL double sterile distilled water and filtered with Whatman No. 1 filter paper after cooling. ACLE was stored at 4 °C for further experiments. $AgNO_3$ (AR grade) was obtained from Himedia Laboratories Pvt. Ltd., Mumbai, India. Ten milliliters of ACLE was carefully measured and added to 90 mL of aqueous solution of $AgNO_3$ (1 mM) in a 250 mL Erlenmeyer flask. The flasks were incubated in the dark at room temperature for the reduction of Ag^+ to Ag^0 nanoparticles for 24 h, resulting in the formation of yellowish-brown to dark brown solution indicating the synthesis of AC-AgNPs.

2.3 Characterization of AC-AgNPs

2.3.1 UV-vis analysis. The bioreduction of $AgNO_3$ to AgNPs was recorded periodically by visual observation of the solution and by measuring the UV-visible spectra of reaction medium using Shimadzu UV-1800 spectrophotometer with a wavelength range between 190 and 900 nm. The progress of the reaction between Ag^+ and the ACLE was monitored by UV-visible spectra of AC-AgNPs in aqueous solution with different reaction times of 15, 30, 45 and 60 min with Milli-Q water as a reference. After 6 h of incubation, the AC-AgNPs were concentrated by repeated centrifugation of the reaction mixture at 10 000g for 10 min and their pellets were redispersed in Milli-Q water to ensure complete separation of AgNPs. The supernatant was replaced each time and the pellet was stored at −20 °C for optical measurements.

2.3.2 FTIR analysis. FTIR measurements were done to investigate AgNPs associated molecules. The solid residue obtained by centrifugation is then washed three times with deionized water to remove any unattached biological moieties to the surface of the nanoparticles that are not responsible for bio-functionalization and capping. The resulting residue is then dried completely and ground with potassium bromide (KBr). Powder obtained is used for analysis by a FTIR Spectrometer (PerkinElmer Lx10-8873) in diffuse reflectance mode.

2.3.3 XRD analysis. X-ray-diffraction (XRD) studies were conducted to determine the exact nature of NPs formed. The dried powder of AC-AgNPs was analyzed with X-ray-diffractometer (PANalytical, Xpert, Bruker D8 advance, The Netherlands), operated at 30 kV and 20 mA current with Cu Kα radiation ($\lambda = 1.54$ Å). The scanning range was selected between 10° and 80° (2θ angle). Average size of the AgNPs was calculated from Debye–Scherrer's equation ($D = 0.94\lambda/\beta\cos\theta$), where D is the average size of the crystallite in vertical direction of crystal face, λ is the wavelength of X-ray, β is the full width at half maximum (FWHM) intensity of the peak, and θ is the diffraction angle.

2.3.4 SEM and EDX analysis. Scanning Electron Microscopy (SEM) was done using ESEM (Model: EVO 18; Carl Zeiss, Germany) with the resolution of 1.0 nm at 30 kV, equipped with 20 mm^2 Oxford beds detector. Energy Dispersive X-ray (EDX) analysis was also performed using the same ESEM. The suspension of synthesized AC-AgNPs was dropped on a carbon-coated copper grid and a thin film was prepared. The sample was allowed to dry under a mercury lamp.

2.3.5 TEM analysis. The size and shape of the prepared AgNPs were confirmed using TEM. High-resolution TEM (HRTEM)

images were obtained using Technai-20, Philips instrument operated at 200 kV and beam current of 104.1 A. The sample for this analysis was prepared by coating the aqueous AC-AgNPs on carbon-coated copper grids (300 mesh size) by slow evaporation and then allowed to dry in vacuum at 25 °C for overnight.

2.4 *In vitro* DNA binding study

The interaction between calf thymus DNA (CT-DNA) and AC-AgNPs was studied by UV-vis spectral analysis following Pathak *et al.*[22] Solution of CT-DNA was prepared in Tris–HCl buffer (0.1 M) (pH = 7.2) with 12 h stirring below 4 °C. Absorption experiments were carried out by keeping constant concentration of AC-AgNPs (0.25 mg) whereby varying the CT-DNA concentration (40–320 μL). Spectral changes of AC-AgNPs were monitored by recording UV-visible absorption in the range of 300–600 nm, after adding different concentrations of CT-DNA.

2.5 Antioxidant activity of AC-AgNPs

Antioxidant activity of AC-AgNPs was determined by DPPH and ABTS free radical scavenging assay.

2.5.1 DPPH assay. One milliliter methanolic DPPH (Himedia, Mumbai) solution (0.1 mM) added with 1 mL methanolic solutions of AC-AgNPs (31.25, 62.5, 125, 250 and 500 μg mL^{-1}). The reacting mixture was shaken and incubated in dark for 30 min at 27 ± 2 °C. The absorbance was measured at 517 nm on UV-vis spectrophotometer. Ascorbic acid was used as a standard and the blank was prepared by adding 1.0 mL of methanol to 1.0 mL of 0.1 mM methanolic DPPH. Free radical scavenging activity was calculated using following formula

% scavenging activity

$$= \frac{\text{absorbance of control} - \text{absorbance of sample}}{\text{absorbance of control}} \times 100$$

2.5.2 ABTS assay. ABTS (Himedia, Mumbai) free radical was produced by adding 7 mM ABTS aqueous solution with 2.4 mM potassium persulphate solution for 12 h in the dark at room temperature. The radical was kept in stable state for 2 days before the reaction. Different concentrations of AC-AgNPs were mixed with 2 mL of diluted ABTS solution. The absorbance was recorded at 734 nm after 30 min of incubation at room temperature. The blank was prepared accordingly, without NPs, and ascorbic acid was used as standard. Free radical scavenging activity was calculated using aforementioned formula.

2.6 H$_2$O$_2$ sensing capacity of AC-AgNPs

The H$_2$O$_2$ sensing capacity of green synthesized AC-AgNPs was observed following Mahadevan *et al.* with slight modification.[23] One milliliter of 20 mM H$_2$O$_2$ (CDH Chemicals, New Delhi, India) was added to 3 mL colloidal solution of AC-AgNPs and mixed thoroughly. The initial spectrum of diluted AC-AgNPs solution (with 3 mL Milli Q water) was recorded using the spectrophotometer. The spectral observations of the reacting solution were recorded at regular intervals.

2.7 Photocatalytic activity of AC-AgNPs

The catalytic activity of AC-AgNPs was studied by degrading toxic dye MB under sunlight. MB (AR, MW = 319.86) was procured from CDH chemicals, New Delhi, India and experiment was designed following Rodríguez-Cabo *et al.*[24] The dye solution was prepared by dissolving 1 mg MB in 100 mL deionized water. Ten milligrams of AgNPs were added to 50 mL dye solution and the mixture was stirred magnetically (Spinot, Tarsons) for 45 min in dark before illumination. A control was also prepared without AC-AgNPs and kept under the similar condition. UV-visible spectra and absorption maxima were observed at regular intervals of 15 min to monitor the dye degradation.

3. Results and discussion

3.1 Phytoreduction of silver ions

During a visual observation, the solution of AgNO$_3$ incubated with ACLE showed color changes from colorless to yellowish-brown within 15 min (Fig. 1a). The appearance of reddish-brown color in ACLE treated flask is a clear indication of the formation of AC-AgNPs within 30 min. After long incubation (2 h) it showed brown color which means the complete formation of AgNPs from aqueous ACLE. This color arises due to excitation of surface plasmon resonance (SPR) in metal NPs. In principle, color changes of the reaction mixture are due to the collective vibration of free electrons induced by an electromagnetic field. Changes in the electronic energy level due to excitation of electrons reflect the reduction of Ag$^+$ into Ag^0 which attributes to reddish brown color of synthesized AC-AgNPs in aqueous solution. The reduction of Ag$^+$ occurred due to the water-soluble phytochemicals present in the leaf samples. *A. conyzoides* leaves are reported to be rich in tannins and other phytochemicals such as alkaloids, flavonoids, terpenoids, saponins, cardiac glycosides, resins, steroids, phenols, essential and non-essential amino acids, *etc.*[25,26] Such phytochemicals may act as reducing, capping as well as stabilizing agents. A schematic representation of the possible mechanism of NPs synthesis is shown in Fig. 1b. Nonetheless, further investigations are required to monitor the role of specific molecules involved in the biosynthesis of AgNPs. The reduction mechanism of polyphenols like tannin and tannic acid with AgNO$_3$ may also involve in the phytomediated synthesis of AgNPs.[27] The suggested mechanism of AgNPs biosynthesis involves the formation of intermediate complexes between AgNO$_3$ and phenolic OH groups in hydrolyzable tannins. The complex undergoes oxidation to quinine forms with subsequent reduction of Ag$^+$ to AgNPs.[28] According to Bulut and Ozacar, debonded H-bonds of OH groups present in tannins serves as a chemical reducer, surface stabilizer and template for Ag$^+$ to Ag reaction to occur.[29]

3.2 UV-vis spectral analysis

The spectrophotometric analysis records the optical density or intensity of absorption as a function of wavelength. The UV-vis spectroscopy serves as the most agreeable approach for the characterization of AgNPs and used to determine the concentration of the NPs in aqueous solution. Fig. 1c shows the UV-vis
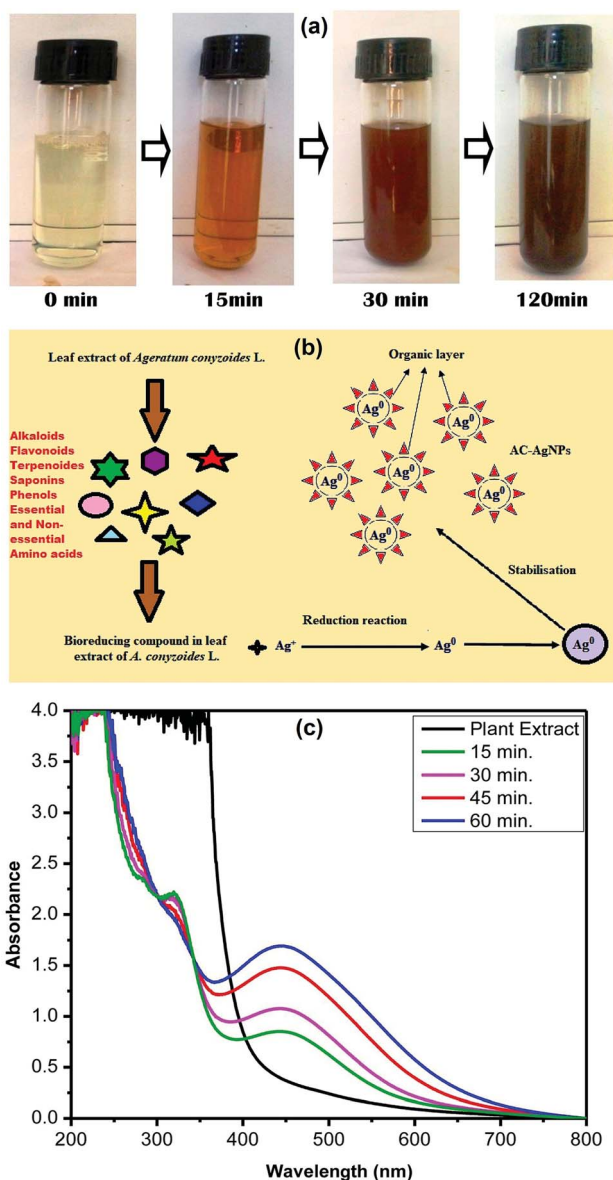
synthesizer. Another weak absorption peak of at 320 nm indicates the presence of several organic compounds and aromatic amino acids which are known to interact with Ag^+.

3.3 FTIR spectral analysis

FTIR spectrum of phytosynthesized AC-AgNPs is shown in Fig. 2a, that reveals the involvement of possible biomolecules and functional groups in AgNPs biosynthesis. The IR-spectrum shows absorption bands at 3440.29, 2358.95, 1613.99, 1383.98, 1074.83 and 699.38 cm^{-1}. The peak at 3440.29 cm^{-1} corresponds to amide N–H stretching. The peak observed at 2358.95 cm^{-1} may be due to C–H stretching of the methylene group. Band at 1383.98 cm^{-1} corresponds to the presence of stretching vibrations of alcohol, ethers, esters, carboxylic acids, and amino acids.[31] Band at 1613.99 cm^{-1} corresponding to the C=O (amide I) and the peak in 1074.83 cm^{-1} can be attributed to the stretching vibration of the C–OH bond from proteins in the plant extract.[31,32] The functional groups like C=O, N–H, and C–H groups present in the ACLE might be responsible for bioreduction of Ag^+ to AgNPs. Observed peaks considered as major

Fig. 1 (a) Visual identification of AgNPs synthesized by ACLE recorded at different functional time viz. 0 min, 15 min, 30 min and 2 h. (b) The schematic diagram for a possible mechanism of ACLE mediated NPs synthesis. (c) UV-visible absorbance spectra of synthesized AgNPs from ACLE at different time intervals.

spectra of the aqueous plant extracts with 1 mM $AgNO_3$ solution. After 15 min of reaction time at room temperature (33 °C), a characteristic plasmon band with λ_{max} appeared at 443 nm. Adsorption of materials unto the surface of the metal nanoparticles leads to excitation of the surface plasmon. It causes scattering of strong light by an electric field where resonance occurs, proceeding in the appearance of strong SPR bands.[30] Fig. 1c demonstrates that the intensity of the peaks continued to increase at various time intervals up to 60 min with the same absorption maxima. AgNPs produced from ACLE were observed to be very stable in the solution with no evidence of flocculation and agglomeration even 2 months after their synthesis which validates the potential application of ACLE as AgNPs
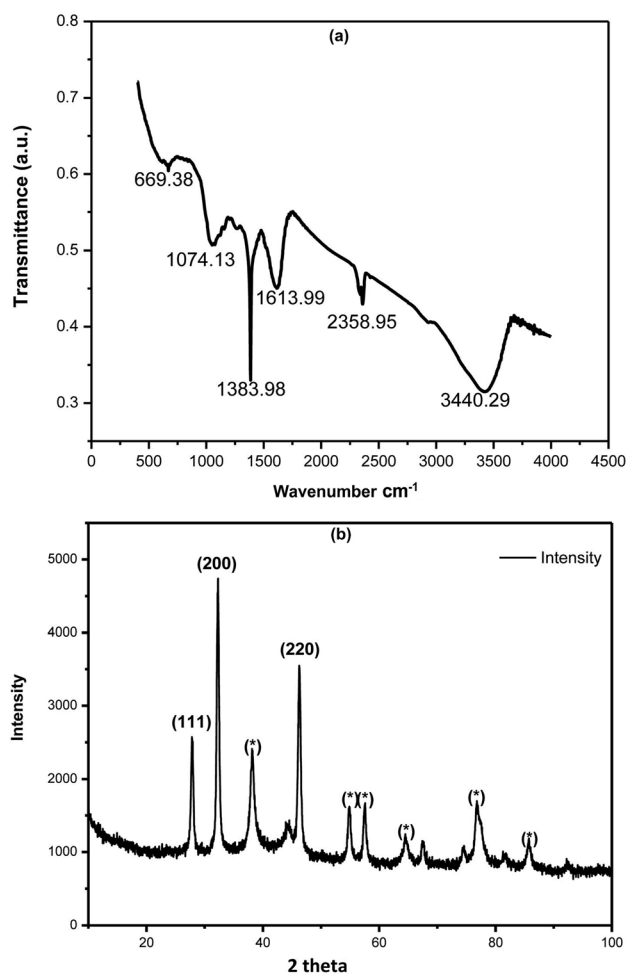

Fig. 2 (a) FTIR spectrum of green synthesized AgNPs using ACLE. (b) XRD pattern of green synthesized AgNPs exhibiting the facets of crystalline Ag.

functional groups in different chemical classes such as poly-saccharides, flavonoids, triterpenoids, and polyphenols.[33]

3.4 XRD analysis

The XRD profile of synthesized AC-AgNPs is depicted in Fig. 2b, which confirms the existence of Ag colloids in the sample. The Braggs reflections were observed in the XRD pattern at $2\theta = 28$, 32 and 46 that clearly indicates the presence of (111), (200) and (220) sets of lattice plane, respectively. Peaks pattern can be readily indexed to a face-centered cubic (fcc) structure of silver (JCPDS, file no. 893722).[34] XRD pattern of present investigation revealed the small particle size, and crystalline nature of

synthesized AC-AgNPs. Some additional unassigned peaks were also noticed in the vicinity of the characteristic peaks suggesting the crystallization of bioorganic phase on the surface of NPs.[35] The average size of NPs was calculated using the Debye–Scherrer equation was 35 nm. The cubic nature of phytosynthesized AgNPs are also reported from several studies.

3.5 SEM and EDX analysis

SEM analysis was employed to visualize the morphology and size of AgNPs. Different magnifications of SEM images are shown in Fig. 3a and b, which confirms the formation of homogenous and relatively spherical AC-AgNPs. The elemental
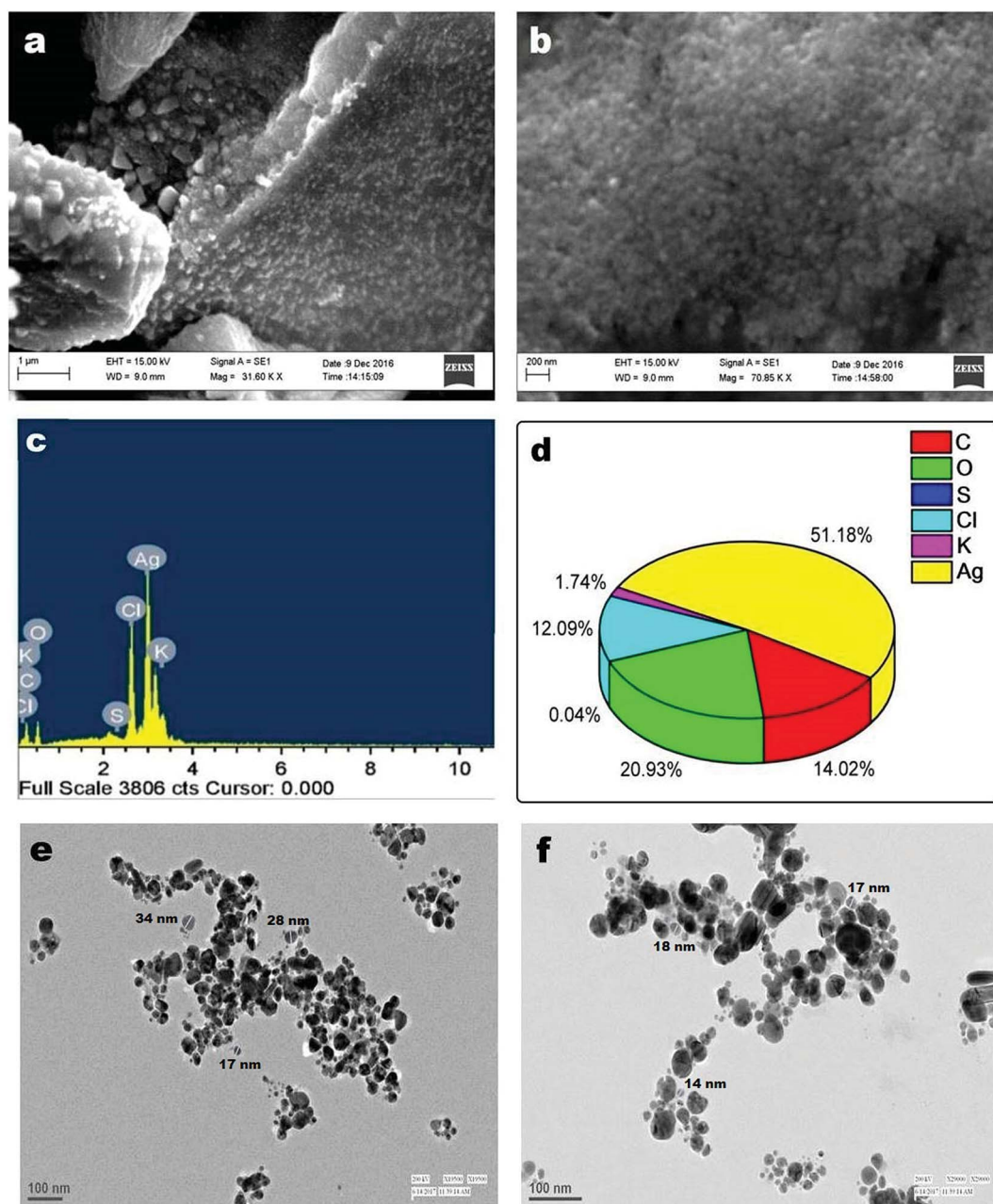

Fig. 3 (a and b) SEM images of AgNPs synthesized from ACLE. (c) EDX spectrum of synthesized AgNPs from ACLE. (d) Quantitative analysis of EDX data. (e and f) TEM images of synthesized AgNPs from ACLE.
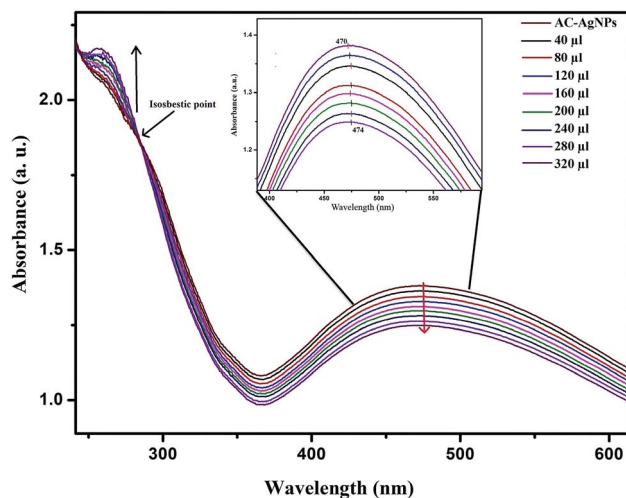
Fig. 4 UV-vis absorption spectra of AC-AgNPs with CT-DNA at various concentrations of CT-DNA (40–320 μL).

composition of NPs was analyzed through energy dispersive X-ray analysis (EDX). Fig. 3c represents the EDX spectrum showing the major elemental peak at 3 keV which is specified for metallic silver. Other small peaks of C, O, S, Cl and K were also arisen due to the capping of AgNPs by biomolecules of ACLE. Quantitative estimation reveals elemental Ag with the higher weight percentage of 51.18%, whereas, O, C, Cl, K, and S having weight percentages of 20.93%, 14.02%, 12.09%, 1.74% and 0.04%, respectively (Fig. 3d).

3.6 TEM analysis

The images obtained from transmission electron microscopy (TEM) of AC-AgNPs are shown in Fig. 3e and f. TEM images elucidate the formation of isotropic and nearly spherical nanoparticles which is in agreement with the shape from the SPR band in the UV-vis spectra. From the TEM image, the particle size range was measured between 14–48 nm which was in accordance with the particle size calculated from the XRD spectrum.

3.7 *In vitro* DNA binding capability

UV-vis spectral titration is one of the important tools for determining the DNA binding capacity of compounds. Prior to addition with AC-AgNPs, the stability of CT-DNA was examined at room temperature with intervals of 15 min and the absorption peak was monitored for 1 h. The experiment was carried out keeping the concentration of AC-AgNPs constant to which CT-DNA was gradually added. Successive binding of AC-AgNPs with CT-DNA resulted to decrease in absorption with significant, though minor, bathochromic effect or red-shift (470 nm to 474 nm) in spectrum indicating
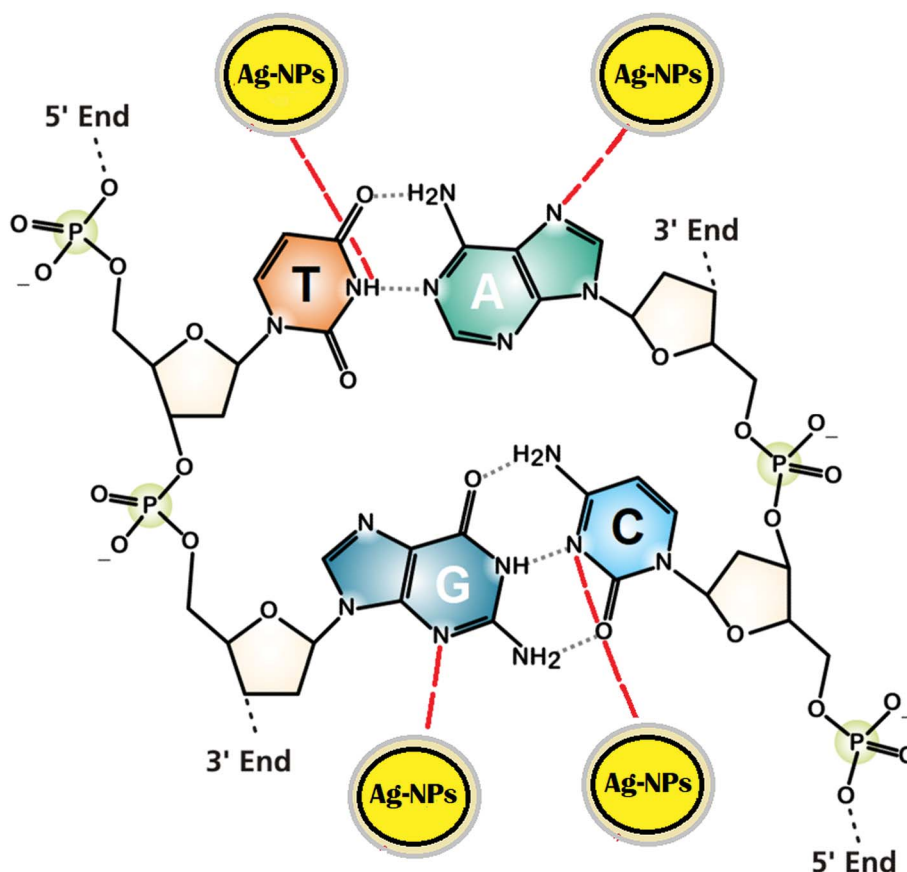

Fig. 5 Possible binding site for AC-AgNPs in the CT-DNA.

that AgNPs preferably interact with DNA (Fig. 4). Absorption spectra of CT-DNA showed a hyperchromic effect with an isosbestic point, which indicates a very strong interaction between NPs and CT-DNA.[9] Only a few studies on the interactive mechanism of some small molecules and DNA have been reported where electrostatic binding, groove binding, and intercalation are the three suggested modes of interactions.[8,22] Fig. 5 depicts the possible hydrogen bonding sites of CT-DNA with bioorganic capping molecules bound to AC-AgNPs, where N_7 atoms of guanine and adenine bases and N_3 atoms of cytosine and thymine bases are involved in interaction.[36]

3.8 Antioxidant activity of AC-AgNPs

DPPH and ABTS radical scavenging assay are relatively quick and sensitive methods of evaluating the antioxidant activity of particular compounds. DPPH is a stable free radical having violet to blue color that converts into a diamagnetic molecule (light yellow) when reacts with electron or hydrogen molecules. The intensity of color change depends on concentration and nature of sample.

Dose dependent free radical scavenging activity is shown in Fig. 6a and b. The DPPH radical inhibition was found between 53.61 ± 0.01 to 89.82 ± 0.017 percent in 31.25 to 500 µg mL^{-1} concentration of AC-AgNPs, while the ascorbic acid produced inhibition of 75.64 ± 0.08 to 98.94 ± 0.03 (Fig. 6a). Similarly, percent ABTS radical inhibition was found 40.16 ± 0.13 to 81.1 ± 0.13 in 31.25 to 500 µg mL^{-1} concentrations of AC-AgNPs. However, at the same concentration, ascorbic acid displayed inhibition activity of 38.39 ± 0.05 to 88.09 ± 0.1 (Fig. 6b). The free radical scavenging activities of AC-AgNPs are similar to some previous reports.[31,37] The functional groups of the bioreductant molecules originated from ACLE, adhered to the surface of the particles have been attributed for the free radical scavenging activity of the AC-AgNPs.[38]

3.9 H$_2$O$_2$ sensing capacity of AC-AgNPs

Fig. 7 shows the changes in the optical characteristics of AC-AgNPs with time due to the addition of 20 mM H$_2$O$_2$. As shown in the inset of Fig. 7, the brown color (vial a) gradually disappeared and finally became colorless (vial c) after 25 min. The decreasing absorbance was observed with the time of reaction, and eventually, the characteristic SPR peak of silver disappeared. No change in the intensity of the SPR absorbance was observed in control without H$_2$O$_2$. The change in color and concentration of the AgNPs solution and decrease of the SPR peak was attributed to the ability of silver to catalyze the decomposition of H$_2$O$_2$.[4,14,39] Mohan et al. suggested that the addition of AgNPs to H$_2$O$_2$ leads to the formation of free radicals which initiate the degradation of the AgNPs.[40] Subsequently, Ag^0 oxidizes to Ag$^+$ and thus caused a decrease in absorbance. In accordance with Bera and Raj, the redox potential of H$_2$O$_2$/H$_2$O couple (1.763 V in acidic medium) or H$_2$O$_2$/OH$^-$ couple (0.867 V in basic medium) is higher than that of the Ag(I)/Ag couple (0.8 V) and H$_2$O$_2$ can efficiently oxidize AgNPs in both acidic and basic
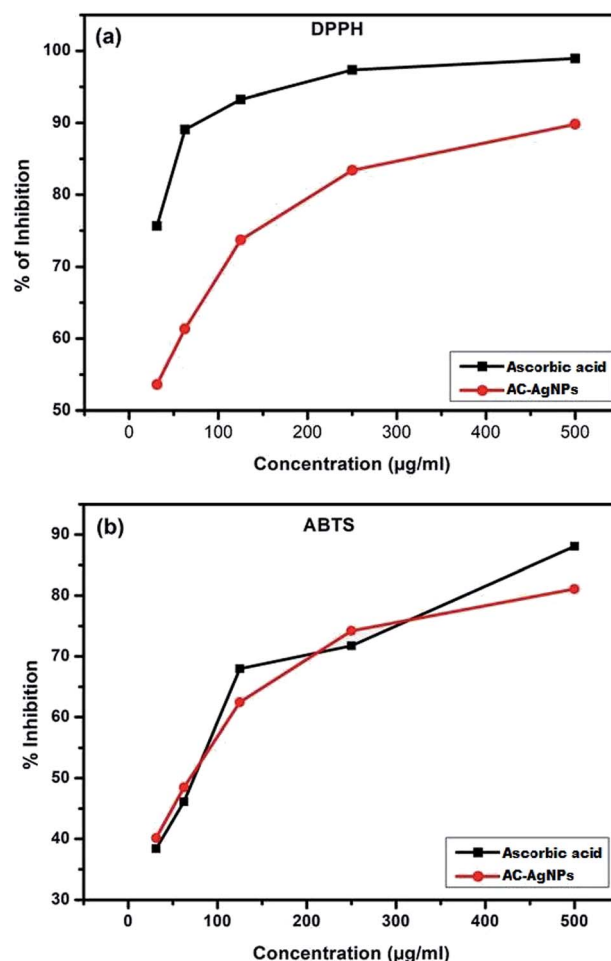
Fig. 6 (a) DPPH free radical scavenging activity of AC-AgNPs. (b) ABTS free radical scavenging assay of AC-AgNPs.

medium.[41] These findings suggest the successful use of AgNPs to detect the concentration of H$_2$O$_2$ present in various unknown samples.
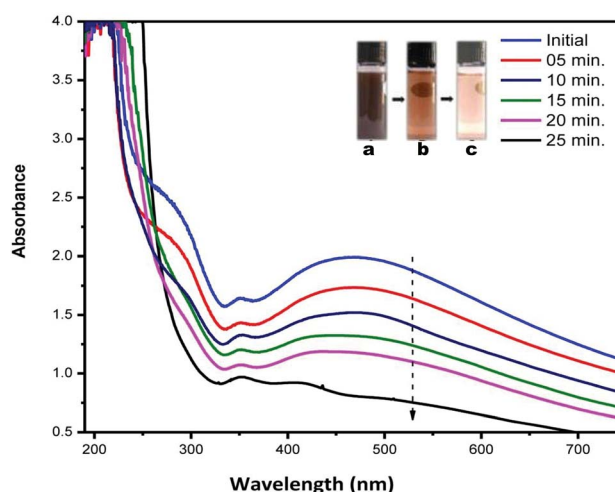
Fig. 7 UV-visible absorbance spectra of AC-AgNPs solution recorded at different time interval after the addition of H$_2$O$_2$ (inset: reacting solution (a) initial (b) after 15 min (c) after 25 min).
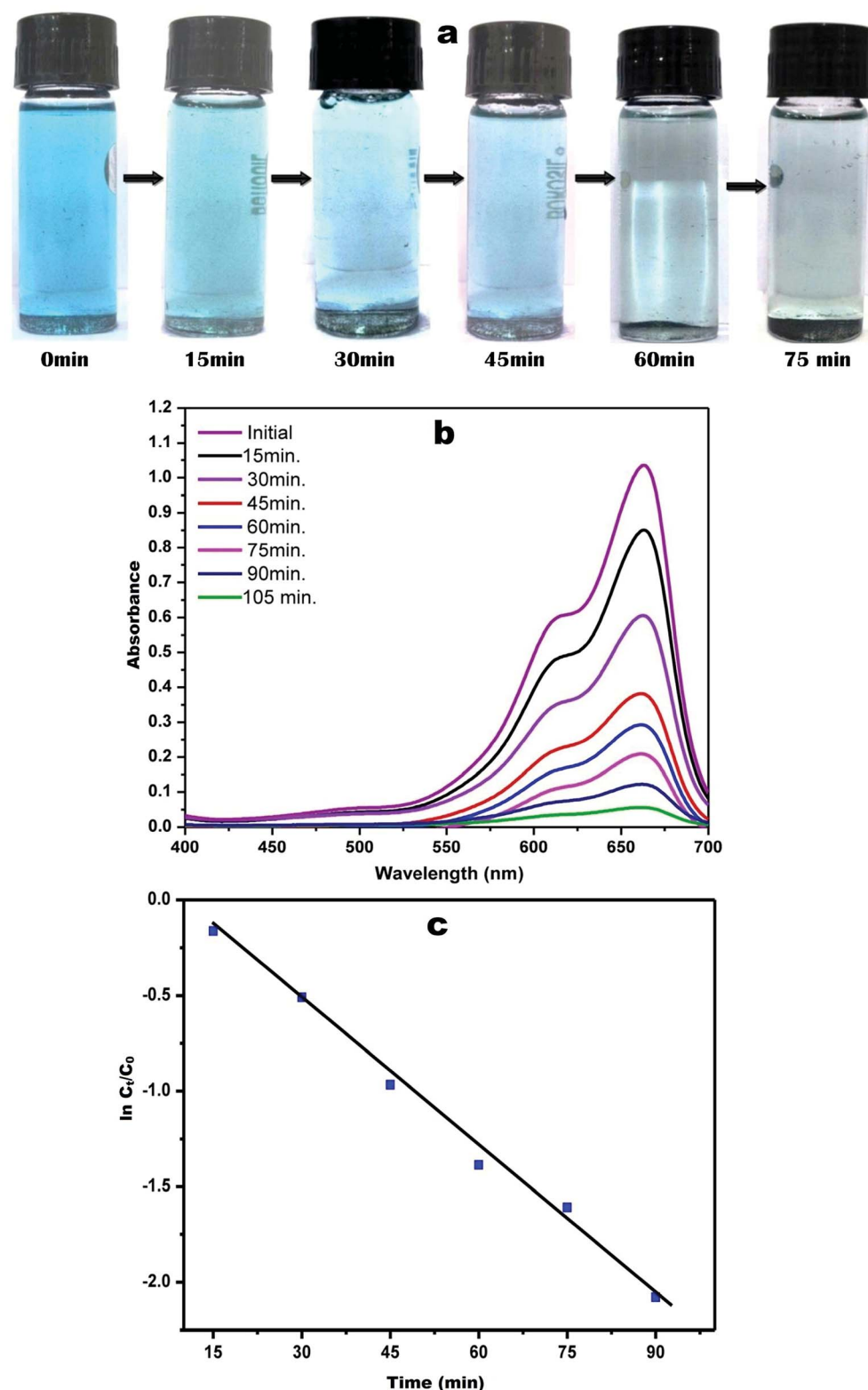
Fig. 8 (a) Visual observation of MB degradation by AC-AgNPs at different time intervals. (b) UV-vis absorbance spectra at 15 min intervals showing reduction of MB in presence of AC-AgNPs. (c) Plot of $\ln(C_t/C_0)$ vs. time (min) for catalytic degradation of MB.

3.10 Photocatalytic activity of AC-AgNPs

Methylene blue, also known as methyl thioninium chloride is a basic aniline dye with molecular formula $C_{16}H_{18}C_1N_3S$. It has a blue color in an oxidized state and upon reduction turns colorless forming leuco-methylene blue. Despite several uses in staining and medication, MB has been reported for severe CNS toxicity and carcinogenicity.[41] The catalytic activity of the green

synthesized AC-AgNPs was studied by the degradation of MB under solar light. Fig. 8a indicates the visual detection of MB degradation by a gradual change in the color of dye solution from blue to colorless. The characteristic absorption maximum for MB was peaked at 663 nm. The degradation of MB in the presence of green synthesized AC-AgNPs was confirmed by the gradual decrease of the peak intensity during 2 h of exposure in sunlight shown in Fig. 8b. The control exhibited no change in coloration until the end of exposure time. AC-AgNPs exhibited rapid photocatalytic activity on their surface, which is stabilized by phytomolecules. The photocatalytic decolorization efficiency of AC-AgNPs for MB was calculated in terms of dye degradation (%) following the equation of Alshehri et al. with slight modification.[19]

$$\text{Dye degradation (\%)} = [1 - C_t/C_0]100$$

where C_0 is the initial concentration of the MB solution at $t = 0$ and C_t is the concentration of the dye solution after a certain reaction time of exposure to sunlight. The concentrations of MB were measured by taking the value of absorbance at 663 nm in the UV-vis spectra as the concentration is directly proportional to the absorbance value. In a similar type of works Cordia dichotoma, Zanthoxylum armatum and Morinda tinctoria leaf extracts showed maximum degradation of MB after 6, 24 and 72 h, respectively.[42–44] Whereas, in the present study, it is clearly indicated in the plot that MB was degraded 50 and 100% within 37 and 105 min, respectively. Kinetic analysis is one of the most significant methods of defining reaction pathways. A linear plot (slope: −0.022) of $\ln(C_t/C_0)$ versus time for catalytic reduction of MB by AC-AgNPs is depicted in Fig. 8c, which exhibits pseudo-first-order kinetics. The degradation rate constant value of MB is calculated 2.8×10^{-2} min^{-1}. The regression coefficient ($R^2 = 0.99$) confirmed that the photocatalytic degradation of MB followed the Langmuir–Hinshelwood kinetic model.[19] The electrons are excited during sunlight when the photons hit the surface of NPs present in the colloidal mixture. The dissolved molecules of oxygen in the solution accept the excited electrons from the surface of NPs and converted into oxygen anion radicals. These radicals convert the organic dye into simpler organic molecules leading to the rapid degradation of MB. Therefore, the biosynthesized AC-AgNPs may act as a stable and efficient green catalyst for the degradation of MB under visible light.

4.   Conclusion

This study demonstrated a facile, eco-friendly and green approach to synthesize AgNPs using ACLE, taking advantage of the natural reducing and capping ability of its constituent compounds. Phytosynthesis was found to be competent in terms of reaction time as well as the stability of the synthesized AgNPs that did not include external stabilizers/reducing agents. Absorption spectrum with SPR peak at 443 nm confirmed the formation of stable AgNPs in the reaction mixture. FTIR spectrum showed that the phyto-molecules present in the aqueous extract of AC are responsible for reducing $AgNO_3$ and capping the active molecules in the AgNPs. The green synthesized AC-AgNPs were found to have a crystalline nature with face-centered cubic (FCC) geometry as studied by XRD. The spherical shape of the NPs with the size range of 14–48 nm was confirmed by SEM and TEM. EDX confirmed the structural and elemental composition of AC-AgNPs. The ability of AgNPs to interact with CT-DNA, showing free radical scavenging activity, H_2O_2 sensing activities are worth remarkable in bionanotechnology and nanomedicine sciences. The outstanding photocatalytic activity of the AgNPs was primarily ascribed to their high photo-degradation capacity for MB. Thus, AC-AgNPs can be exploited for degradation and conversion of industrial pollutants like free radicals and hazardous dyes into harmless mineral compounds.

Conflicts of interest

Authors declare no conflict of interest.

Abbreviations

ACLE	Ageratum conyzoides L. leaf extract
AgNPs	Silver nanoparticles
AC-AgNPs	Ageratum conyzoides L. mediated silver nanoparticles
SPR	Surface plasmon resonance
UV-vis	UV-visible spectrophotometer
FTIR	Fourier transform infrared spectrum
SEM	Scanning electron microscopy
TEM	Transmission electron microscopy
XRD	X-ray diffraction
EDX	Energy dispersive X-ray
H_2O_2	Hydrogen peroxide
MB	Methylene blue
DPPH	2,2-Diphenyl-1-picrylhydrazyl
ABTS	2,2′-Azino-bis-3-ethylbenzothiazoline-6-sulphonic acid
CT-DNA	Calf thymus DNA
$AgNO_3$	Silver nitrate

Acknowledgements

References

1 V. S. Ramkumar, A. Pugazhendhi, K. Gopalakrishnan, P. Sivagurunathan, G. D. Saratale, T. N. B. Dung and E. Kannapiran, Biotechnol. Rep., 2017, 14, 1–7.

2 M. S. Akhtar, J. Panwar and Y. S. Yun, ACS Sustainable Chem. Eng., 2013, 6, 591–602.

3 S. Ahmed and S. Ikram, *J. Nanomed. Nanotechnol.*, 2015, **6**(4), 309.

4 P. Kuppusamy, M. M. Yusoff, G. P. Maniam and N. Govindan, *Saudi Pharm. J.*, 2016, **4**, 473–484.

5 F. Eya'aneMeva, M. L. Segnou, C. O. Ebongue, A. A. Ntoumba, P. B. E. Kedi, V. Deli, M. A. Etoh and E. M. Mpondo, *Rev. Bras. Farmacogn.*, 2016, **26**, 640–646.

6 J. J. Vijaya, N. Jayaprakash, K. Kombaiah, K. Kaviyarasu, L. J. Kennedy, R. J. Ramalingam, H. A. Al-Lohedan, V. M. Mansoor-Ali and M. Maaza, *J. Photochem. Photobiol., B*, 2017, **177**, 62–68.

7 J. Y. Song and B. S. Kim, *Biosyst. Eng.*, 2009, **32**, 79–84.

8 A. P. Ribeiro, S. Anbu, E. C. Alegria, A. R. Fernandes, P. V. Baptista, R. Mendes, A. S. Matias, M. Mendes, M. G. da Silva and A. J. Pombeiro, *Biomed. Pharmacother.*, 2018, **101**, 137–144.

9 K. Sonia, S. Kukreti and M. Kaushik, *J. Photochem. Photobiol., B*, 2019, **194**, 158–165.

10 K. Tagad, H. U. Kim, R. C. Aiyer, P. More, T. Kim, S. H. Moh, A. Kulkarni and S. G. Sabharwal, *RSC Adv.*, 2013, **45**, 22940–22943.

11 L. Subramanian, T. Sabu and K. Obey, *International Journal of Biosensors & Bioelectronics*, 2017, **2**, 22.

12 Q. Wang and Y. Yun, *Microchim. Acta*, 2013, **180**, 261–268.

13 R. Liu, Y. Wei, J. Zheng, H. Zhang and Q. Sheng, *Chin. J. Chem.*, 2013, **3**, 1519–1525.

14 S. Raja, V. Ramesh and V. Thivaharan, *Arab. J. Chem.*, 2017, **10**, 253–261.

15 B. Kumar, K. Smita and L. Cumbal, *Nanotechnol. Rev.*, 2016, **5**, 521–528.

16 A. Turunc, R. Binzet, I. Gumus, G. Binzet and H. Arslan, *Mater. Chem. Phys.*, 2017, **202**, 310–319.

17 A. Zabłocka-Godlewska, W. Przystaś and E. Grabińska-Sota, *Water, Air, Soil Pollut.*, 2018, **229**(6), 176, DOI: 10.1007/s11270-018-3829-7.

18 J. H. Shah, M. Fiaz, M. Athar, J. Ali, M. Rubab, R. Mehmood, S. U. U. Jamil and R. Djellabi, *Environ. Technol.*, 2019, **9**, 1–10.

19 A. Alshehri, M. A. Malik, Z. Khan, S. A. Al-Thabaiti and N. Hasan, *RSC Adv.*, 2017, **40**, 25149–25159.

20 L. Okunade, *Fitoterapia*, 2002, **73**, 1–16.

21 A. Egunyomi, I. T. Gbadamosi and M. O. Animashahun, *J. Med. Plants Res.*, 2011, **5**, 5347–5350.

22 S. Pathak, M. K. Ghosh and T. K. Ghorai, *ChemistrySelect*, 2018, **3**, 13501–13506.

23 S. Mahadevan, S. Vijayakumar and P. Arulmozhi, *Microb. Pathog.*, 2017, **113**, 445–450.

24 B. Rodríguez-Cabo, I. Rodríguez-Palmeiro, R. Corchero, R. Rodil, E. Rodil, A. Arce and A. Soto, *Water Sci. Technol.*, 2017, **75**, 128–140.

25 P. A. Wuyep, H. D. Musa, G. C. Ezemokwe, D. D. Nyam and M. D. SilaGyang, *J. Acad. Ind. Res.*, 2017, **6**(3), 32–38.

26 R. Kaur and N. K. Dogra, *International Journal of Pharmaceutical & Biological Archive*, 2014, **5**(5), 33–45.

27 T. Y. Kim, S. H. Cha, S. Cho and Y. Park, *Arch. Pharmacal Res.*, 2016, **39**, 465–473.

28 R. S. Priya, D. Geetha and P. S. Ramesh, *Ecotoxicol. Environ. Saf.*, 2016, **134**, 308–318.

29 E. Bulut and M. Ozacar, *Ind. Eng. Chem. Res.*, 2009, **48**, 5686–5690.

30 T. Kokila, P. S. Ramesh and D. Geetha, *Ecotoxicol. Environ. Saf.*, 2016, **134**, 467–473.

31 A. Saravanakumar, M. M. Peng, M. Ganesh, J. Jayaprakash, M. Mohankumar and H. T. Jang, *Artif. Cells, Nanomed., Biotechnol.*, 2016, **45**, 1165–1171.

32 S. Bhakya, S. Muthukrishnan, M. Sukumaran and M. Muthukumar, *Appl. Nanosci.*, 2016, **6**, 755–766.

33 A. Nabikhan, K. Kandasamy, A. Raj and N. M. Alikunhi, *Colloids Surf., B*, 2010, **79**, 488–493.

34 A. Sudhakar, K. Selvam, M. Govarthanan, B. Senthilkumar, A. Sengottaiyan, M. Stalin and T. Selvankumar, *Int. J. Genet. Eng. Biotechnol.*, 2015, **13**, 93–99.

35 S. Ponarulselvam, C. Panneerselvam, K. Murugan, N. Aarthi, K. Kalimuthu and S. Thangamani, *Asian Pac. J. Trop. Biomed.*, 2012, **2**, 574–580.

36 H. An and B. Jin, *Biotechnol. Adv.*, 2012, **30**, 1721–1732.

37 A. Lateef, M. A. Azeez, T. B. Asafa, T. A. Yekeen, A. Akinboro, I. C. Oladipo, L. Azeez, S. E. Ajibade, S. A. Ojo, E. B. Gueguim-Kana and L. S. Beukes, *J. Taibah Univ. Sci.*, 2016, **10**, 551–562.

38 T. C. Shekhar and G. Anju, *Am. J. Ethnomed.*, 2014, **4**, 244–249.

39 B. Ajitha, Y. A. K. Reddy, P. S. Reddy, H. J. Jeon and C. W. Ahn, *RSC Adv.*, 2016, **6**, 36171–36179.

40 S. Mohan, O. S. Oluwafemi, S. C. George, V. P. Jayachandran, F. B. Lewu, S. P. Songca, N. Kalarikkal and S. Thomas, *Carbohydr. Polym.*, 2014, **106**, 469–474.

41 R. K. Bera and C. R. Raj, *J. Photochem. Photobiol., A*, 2013, **270**, 1–6.

42 I. Mohmood, C. B. Lopes, I. Lopes, I. Ahmad, A. C. Duarte and E. Pereira, *Environ. Sci. Pollut. Res.*, 2013, **20**, 1239–1260.

43 M. Vanaja, K. Paulkumar, M. Baburaja, S. Rajeshkumar, G. Gnanajobitha, C. Malarkodi, M. Sivakavinesan and G. Annadurai, *Bioinorg. Chem. Appl.*, 2014, DOI: 10.1155/2014/742346.

44 K. Jyoti and A. Singh, *Int. J. Genet. Eng. Biotechnol.*, 2016, **14**, 311–317.